Structural stability, electronic structure, and magnetic properties of mixed-valence ACr_3O_8 phases (A=Na, K, Rb)

R. Vidya,* P. Ravindran, P. Vajeeston, H. Fjellvåg, and A. Kjekshus
Department of Chemistry, University of Oslo, Box 1033 Blindern, N-0315 Oslo, Norway
(Received 11 January 2005; revised manuscript received 5 April 2005; published 5 July 2005)

The structural stability, electronic structure, and magnetic properties are studied for ACr_3O_8 (A=Na, K, Rb; Cr in two formally different valence states) using accurate density-functional calculations. The calculations show that at 0 K and high pressures $NaCr_3O_8$ remains a ferromagnetic insulator whereas KCr_3O_8 and $RbCr_3O_8$ undergo an antiferromagnetic-insulator-to-ferromagnetic-insulator transition, the transition pressure decreasing with increasing radius of A^+ from KCr_3O_8 to $RbCr_3O_8$. Indirect Cr1-to-Cr1 exchange interaction via two intervening oxygen atoms is the origin of the antiferromagnetism. The calculated structural parameters are consistent with the experimental values, actual deviations being discussed.

DOI: 10.1103/PhysRevB.72.014411 PACS number(s): 78.20.Ls, 78.20.Ci

I. INTRODUCTION

Compounds with mixed-valent transition-metal ions are interesting as they exhibit exotic properties such as charge ordering, high-temperature superconductivity, and colossal magnetoresistance (CMR). Since the discovery of CMR, a lot of attention has been paid to mixed-valent manganese compounds. Most frequently studied are 3*d* transition-metal oxides with Mn, Fe, Co, or Cu atoms. Cr substitution for Mn in $Pr_{0.5}Ca_{0.5}Mn_{1-x}Cr_xO_3$ (x=0.02) is found[1] to destroy charge ordering and induces a semiconductor-to-metal transition with only compositional means (viz., without the application of a magnetic field). It may therefore be of interest to study oxides containing mixed-valent Cr. In most studies on mineralogy and petrology of mantle rocks, Cr appears to take only the trivalent state whereas all formal valence states from Cr^{II} to Cr^{VI} are known for man-made compounds. However, Cr^{III} and Cr^{VI} are by far the most common chromium valences for oxides, typically in octahedral and tetrahedral coordination, respectively. For example, Cr has octahedral environment and valence III in spinel-type oxides and tetrahedral environment and valence VI in chromates. In the ACr_3O_8 (A=Na, K, Rb) compounds considered here, Cr takes both octahedral and tetrahedral coordination with formal ionic valence states believed to be Cr^{3+} and Cr^{6+}. Hence a detailed study of the valence states, electronic structures, and magnetic properties of these compounds is of considerable interest.

II. STRUCTURAL ASPECTS

The crystal structure of ACr_3O_8 (A=Na, K, Rb) is summarized in Table I and depicted in Fig. 1. X-ray powder diffraction studies[2,3] have revealed that the three compounds are isostructural and crystallize in the monoclinic space group $C2/m$. The $ACr1^oCr2_2^tO_8$ structure consists of two types of Cr atoms arranged in octahedral (o) and tetrahedral (t) environments. There are three crystallographically different O atoms. Cr1 forms six bonds with O atoms, two with O1 and four with O3, in a fairly regular octahedral arrange-

TABLE I. Optimized structural parameters, bulk modulus (B_0), and the derivative of bulk modulus (B_0') for ACr_3O_8 (A=Na, K, Rb). Space group $C2/m$: A and Cr1 in positions 2*a* (0,0,0) and 2*c* (0,0,1/2), respectively, Cr2, O1, and O2 in 4*i*, and O3 in 8*i*. Values given in parentheses refer to experimental data quoted from Ref. 3.

Compound	Unit cell (Å or deg)	Atom	x	y	z	B_0 (GPa)	B_0'
$NaCr_3O_8$	a=8.6223 (8.4957)	Cr2	0.6386 (0.6360)	0	0.2731 (0.2709)	36.56	5.43
	b=5.5249 (5.4763)	O1	0.2277 (0.2256)	0	0.5562 (0.5574)		
	c=6.9214 (6.7991)	O2	0.7158 (0.7118)	0	0.0628 (0.0616)		
	β=90.347 (91.412)	O3	0.0256 (0.0235)	0.2451 (0.2461)	0.2999 (0.3000)		
KCr_3O_8	a=8.8965 (8.5716)	Cr2	0.6385 (0.6248)	0	0.2958 (0.2919)	29.38	4.96
	b=5.4633 (5.4625)	O1	0.2091 (0.2279)	0	0.5699 (0.5591)		
	c=7.8733 (7.6234)	O2	0.6840 (0.6863)	0	0.0984 (0.0884)		
	β=93.493 (95.199)	O3	0.0362 (0.0162)	0.2558 (0.2509)	0.3289 (0.3079)		
$RbCr_3O_8$	a=8.9135 (8.6162)	Cr2	0.6347 (0.6265)	0	0.3028 (0.2994)	26.27	3.84
	b=5.4757 (5.4584)	O1	0.2103 (0.2224)	0	0.5688 (0.5596)		
	c=8.1557 (7.9612)	O2	0.6751 (0.6769)	0	0.1111 (0.1021)		
	β=94.657 (95.813)	O3	0.0373 (0.0125)	0.2552 (0.2599)	0.3356 (0.3194)		

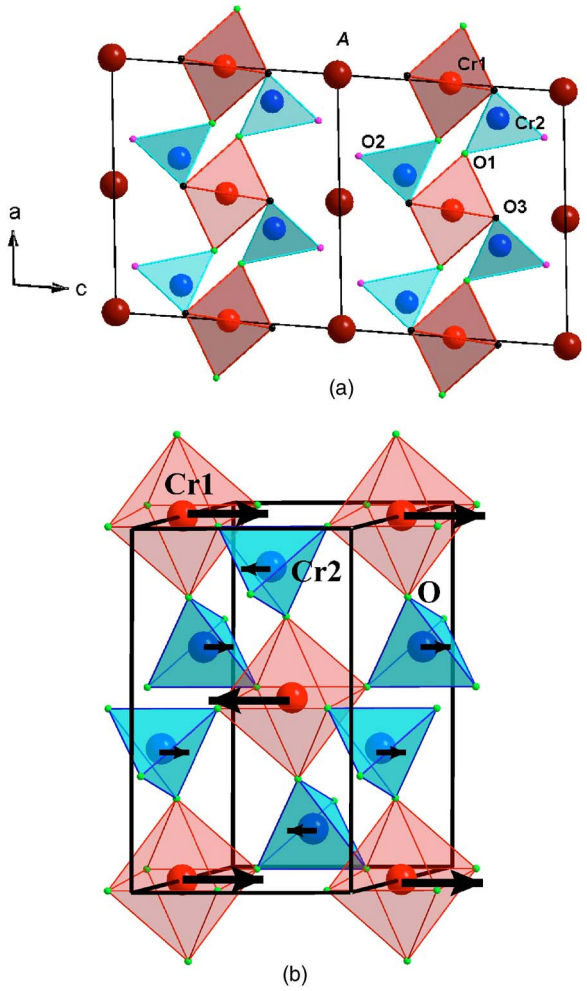

FIG. 1. (Color online) (a) Crystal structure of ACr_3O_8 (A=Na, K, Rb), viewed along [010]. Crystallographically different atoms are labeled on the illustration; see also Table I. Note the distinct Cr_3O_8 layers. (b) The antiferromagnetic (AF) configuration of Cr2 is indicated by arrows; the size is related to the outcome of the calculations. A ions are omitted.

ment. Similarly, Cr2 takes a fairly regular tetrahedral coordination, forming one bond each with O1 and O2 and two bonds with O3. The octahedra and tetrahedra are arranged in layers parallel to the a,b plane by corner sharing. The thus generated layers are held together by the alkali-metal cations which have ten nearest oxygen neighbors. The expansion of the c axis on going from A=Na to Rb in the ACr_3O_8 series is mainly due to the increased size of A^+.

III. COMPUTATIONAL DETAILS

The results presented here are based on density-functional theory (DFT) calculations according to the projected augmented plane-wave[4] (PAW) method as implemented in the VASP code (Vienna *ab initio* simulation package).[5] In this approach the valence orbitals are expanded as plane waves and the interactions between the core and valence electrons are described by pseudopotentials. The optimization of the atomic geometry is performed via a conjugate-gradient algorithm by minimization of the forces and stresses acting on the system. During the simulations, atomic coordinates and axial ratios are allowed to relax for different volumes of the unit cell. These parameters are changed iteratively so that the sum of the lattice energy and the electronic free energy converges to a minimum value. The ground state is calculated exactly for each set of atomic positions and the electronic free energy is taken as the quantity to be minimized. The experimental structural parameters[3] are used as the initial input. Convergence minimum with respect to atomic shifts is assumed to have occurred when the energy difference between two successive iterations is less than 10^{-7} eV f.u.$^{-1}$ and the forces acting on the atoms are less than 1 meV Å^{-1}. The generalized-gradient approximation[6] (GGA) is used to obtain accurate exchange and correlation energies for a particular atomic configuration. The calculations were carried out using a $4\times8\times8$ **k**-point Monkhorst-Pack grid, equivalent to 64 **k** points in the irreducible Brillouin zone. A further increase in the number of **k** points proved to have negligible effect on the total energy. A plane-wave energy cutoff of 550 eV was used in all calculations. In order to avoid ambiguities in the free-energy results we have used same energy cutoff and **k**-point density in all calculations. The structural optimizations were performed in paramagnetic (P), ferromagnetic (F), and antiferromagnetic (AF) configurations for all the three compounds. We have calculated the total energy of the compounds as a function of volume for ten different volumes, fitted the results to the so-called universal equation of state,[7] and therefrom extracted the bulk modulus (B_0) and its pressure derivative (B_0').

IV. RESULTS AND DISCUSSION

A. Structural optimization

The results discussed in the following sections refer to KCr_3O_8 unless otherwise specifically mentioned. The structural optimization in the P, F, and AF configurations shows that the AF configuration has the lowest total energy and represents accordingly the ground state for KCr_3O_8 (Fig. 2). This is in agreement with the magnetic susceptibility data[8,9] which show AF ordering below T_N (Néel temperature) $=125\pm4$ K. The calculations show that $RbCr_3O_8$ also has an AF ground state whereas $NaCr_3O_8$ has a F ground state. The optimized lattice parameters and atomic positions along with the experimental values are given in Table I, showing reasonably good agreement between the two sets of data. The calculated cell parameters agree well for $NaCr_3O_8$, but for KCr_3O_8 and $RbCr_3O_8$ the unit-cell parameters are up to some 3.8% larger than the experimental values. The PAW method with the GGA generally gives up to 3% overestimated volumes in some cases.[10] In order to check the deviations between the computational and experimental structural parameters for these compounds, we repeated the calculations with more **k** points, higher energy cutoff, and also including the semicore K p and Cr p states in the valence configuration. None of these calculations significantly changed the values from those listed in Table I. We also carried out a similar set of calculations using the local-density

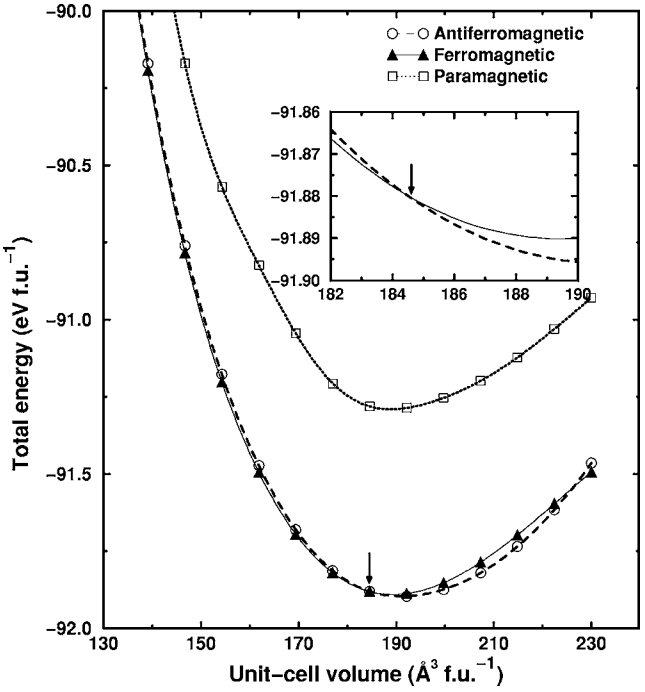

FIG. 2. Calculated unit-cell volume vs total energy for KCr_3O_8 in different magnetic configurations. The arrows indicate the antiferromagnetic-to-ferromagnetic transition.

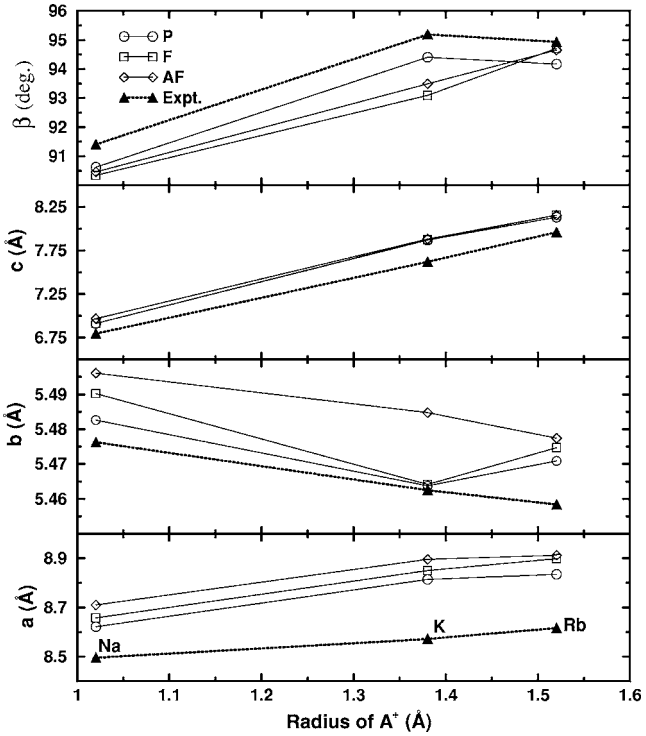

FIG. 3. Calculated unit-cell parameters for ACr_3O_8 as function of the radius of A^+ (standard values). Open and closed symbols represent calculated and experimental values, respectively. Note the enlarged scale along b.

approximation (LDA) instead of the GGA. In this case, the obtained equilibrium parameters are up to 3.6% underestimated.

In order to check the effect of the Cr PAW potential on the lattice parameters we also carried out test calculations with different potentials for CrO_2, which is an archetype for half-metallic ferromagnets. We correctly obtained the F half-metallic ground state and the equilibrium unit-cell volume (see Table II) varied around 2%, viz., well within the limit of the accuracy for DFT calculations. In all calculations the derived magnetic moment per Cr atom in CrO_2 came out as $\sim 2.0\mu_B$ as expected for Cr^{IV} (d^2). Hence the choice of potentials for the constituent elements does not significantly influence the optimized lattice parameters.

As noted earlier, the studied systems have a layered arrangement within a,b planes. It is noteworthy that the largest deviations in lattice parameters between experiment and theory are found precisely for the a direction (3.8% and 3.5% for KCr_3O_8 and $RbCr_3O_8$, respectively). Moreover, for

TABLE II. Optimized unit-cell parameters for CrO_2 using different potentials in the computation: GGA-PBE1 corresponding to pseudopotential for Cr with 3d electrons in the valence state, GGA-PBE2 to pseudocore 2p electrons also in the valence state, and LDA (see Sec. III).

Unit cell	Experiment (Ref. 11)	GGA-PBE1	GGA-PBE2	LDA
a (Å)	4.4190	4.4212	4.4204	4.4348
c (Å)	2.9154	2.9125	2.9135	2.8946
V (Å^3)	56.93	58.13	58.30	55.70

KCr_3O_8 the deviation in a is considerably smaller in the P case (2.8%) than the AF case (3.8%). The significance of the latter finding lies in the fact that the experimental values refer to the P state at room temperature. The variation of b is almost negligible for the P and F states ($\sim 0.02\%$) and somewhat larger for the AF state (0.44%), whereas that for c is more appreciable for all (P, F, and AF) states (3.2–3.4 %; see Fig. 3). From Table III, it is seen that the calculated average bond length Cr1^o-O for the three compounds is some 2% smaller than the experimental value. On the other hand, the calculated and experimental bond lengths Cr2^t-O are almost the same. Cr1 has a finite magnetic moment whereas that for Cr2 is negligible (see Sec. IV B). The strongly bonded tetrahedral $Cr2O_4$ units are not affected by either external pressure or magnetic interactions whereas the octahedral $Cr1O_6$ units are influenced by such perturbations. Hence, the discrepancy between the calculated and experimental lattice parameters may be attributed to the layered structure, the strongly bonded macromolecularlike Cr_3O_8 units within the layers, and/or magnetoelastic effects. As the experimental values refer to room temperature (well above the magnetic transition temperature) and the calculations correspond to 0 K, low-temperature neutron-diffraction studies on the crystal and magnetic structures of these compounds are needed to shed light on this situation.

The change in total energy as a function of unit-cell volume for KCr_3O_8 is shown in Fig. 2. This shows that a transition from the AF to the F state takes place at a pressure of 2.36 GPa, associated with a volume discontinuity of 6.4%. As the energy difference between the AF and F states is

TABLE III. Bond lengths between Cr and O (in Å) in the ground-state configurations of ACr_3O_8.

	$NaCr_3O_8$ (F)		KCr_3O_8 (AF)		$RbCr_3O_8$ (AF)	
Bonds	Calc.	Expt.	Calc.	Expt.	Calc.	Expt.
2 $Cr1^o$-O1	1.94	1.95	1.90	1.95	1.89	1.92
4 $Cr1^o$-O3	1.97	2.00	1.98	2.02	1.93	2.03
1 $Cr2^t$-O1	1.64	1.63	1.62	1.62	1.63	1.63
2 $Cr2^t$-O3	1.69	1.69	1.66	1.66	1.65	1.65
1 $Cr2^t$-O2	1.66	1.65	1.69	1.69	1.68	1.68

small (Table IV), it should be easy for this magnetic transition to occur. Similarly, $RbCr_3O_8$ also undergoes a transition from the AF to the F state at 1.31 GPa, whereas no pressure-induced magnetic transition is revealed for $NaCr_3O_8$ which remains in the F state throughout the pressure range studied.

B. Magnetic properties

We have calculated the total energy for P, F, and AF configurations as well as three different types of ferrimagnetic (Ferri) ordering. However, all Ferri configurations finally ended up with either F or AF solutions. Two different AF arrangements were considered of which that depicted in Fig. 1(b) came out 300 meV f.u.$^{-1}$ lower in energy. We have also calculated the Liechtenstein exchange parameters[12,13] for the Cr atoms based on the formalism implemented in the TBLMTO-47 code[14] and made use of the findings as guidelines to construct the magnetic cell. From the calculated exchange parameters we found that the indirect Cr1-to-Cr1 and Cr2-to-Cr2 interactions via intervening O atoms are AF (magnitudes 64.5 and 0.03 meV, respectively), whereas the corresponding Cr1-to-Cr2, interactions are F (magnitude −2.74 meV). The mutual exchange interaction between the Cr1 and Cr2 sublattices is accordingly very small. Moreover, as Cr2 carries a minor moment (see below) the net macroscopic effect of AF ordering (as assumed in the computational model) or paramagnetic disordering of the Cr2 moments will virtually be the same. Note that the Cr-Cr separation in the compounds ($\geqslant$3.38 Å for KCr_3O_8) exceeds the critical value[15] for direct Cr-Cr interaction. The most likely superexchange-interaction path from Cr1 to Cr1 is via O3 atoms with an O3-O3 separation of 2.72 Å and a Cr1-O3-O3 angle of 133°.

At first sight the calculated magnetic moments (Table V) appear to confirm that Cr1 corresponds to nearly Cr^{III} (d^3) and Cr2 to nearly Cr^{VI} (d^0) in agreement with their octahedral and tetrahedral coordinations.[3] However, a closer investigation of the bonding situation reveals that (see below and Sec. IV D) the assignment of formal valence states to Cr in the studied systems is nontrivial. Owing to the presence of nearly three unpaired d electrons, Cr1 may be concluded as Cr^{III}, but all d electrons from Cr2 are clearly not transferred to the oxygen atoms [as is to be expected for an ideal Cr^{VI} (d^0) state]. A small magnetic moment (Table V) is associated with Cr2, and owing to hybridization interaction between Cr d and O p, the oxygen atoms also possess small magnetic moments. [This leads to total moments in the F state (see Table V) exceeding the simple sum of the moments on Cr1 and Cr2.]

The magnetic moments of Cr1 are lower than the ideal spin-only values owing to strong covalent Cr-O interaction. The old findings of Klemm[8] established Curie-Weiss behavior for KCr_3O_8, but gave a somewhat larger resultant paramagnetic moment [$(4.0–4.2)\mu_B$ f.u.$^{-1}$] than the spin-only paramagnetic moment ($3.72\mu_B$ f.u.$^{-1}$ which "accidentally" coincides with the theoretical spin-only moment for a d^3 configuration) calculated from the total cooperative-magnetic moment for KCr_3O_8 in Table V. Unpublished measurements by Fjellvåg[9] found $\mu_P=(4.05\pm0.03)\mu_B$ and $(4.08\pm0.04)\mu_B$ f.u.$^{-1}$ for $NaCr_3O_8$ and KCr_3O_8, respectively. However, according to Ref. 9 $NaCr_3O_8$ takes an AF arrangement below $T_N=91\pm2$ K (rather than the F arrangement arrived at computationally) and moreover both $NaCr_3O_8$ and KCr_3O_8 have a black appearance (see also Ref. 8). The latter observation suggests that these substances should be metallic rather than semiconducting. A metallic behavior can in this case easily be imagined to arise from nonstoichiometry in the oxygen content of the bona fide samples. There are also other reports[16] of paramagnetic moments in excess of $4\mu_B$ per Cr^{III} for chromic compounds. For example, the related binary oxides Cr_2O_5 and Cr_3O_8 (which also formally are believed to comprise Cr^{3+} and Cr^{6+}) are reported[17] to exhibit AF order-

TABLE IV. Total energy (relative to the lowest-energy state in meV f.u.$^{-1}$) for ACr_3O_8 in P, F, and AF states.

Compound	P	F	AF
$NaCr_3O_8$	680	0	14.5
KCr_3O_8	619	21.4	0
$RbCr_3O_8$	652	21.6	0

TABLE V. Calculated magnetic moment for Cr1 and Cr2 (in μ_B per Cr atom) of ACr_3O_8 in F and AF states. Total refers to the total magnetic moment per formula unit.

	F			AF	
Compound	Cr1	Cr2	Total	Cr1	Cr2
$NaCr_3O_8$	2.451	0.241	2.868	2.391	0.013
KCr_3O_8	2.449	0.228	2.859	2.330	0.016
$RbCr_3O_8$	2.453	0.224	2.857	2.336	0.003

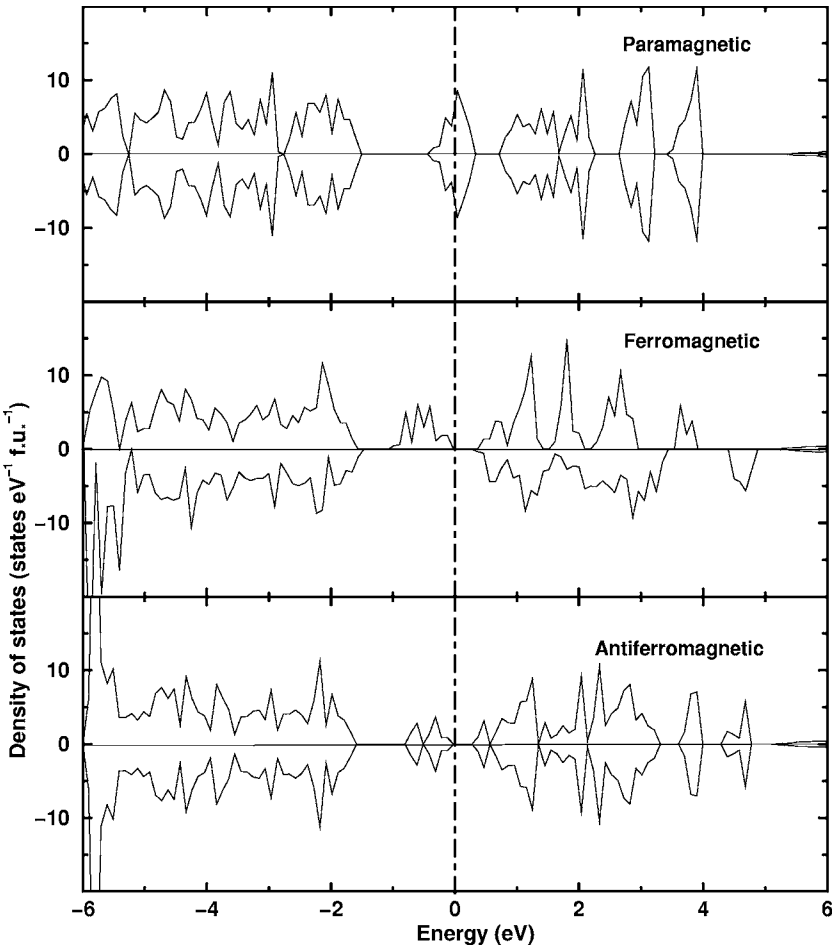

FIG. 4. Total density of states for KCr_3O_8 in different magnetic configurations. The Fermi level (E_F) is indicated by vertical dashed line.

ings at low temperature with paramagnetic moments of $(4.30\pm0.04)\mu_B$ and $(4.35\pm0.02)\mu_B$ f.u.$^{-1}$, respectively.

A number of manganese-containing compounds has been found to transform from an AF insulating (semiconducting) phase to a F metallic phase with an associated CMR effect on application of magnetic fields. The present calculations predict that KCr_3O_8 and $RbCr_3O_8$ stabilize in the F insulating phase (note at 0 K) on application of a sufficiently large field. Transport-property studies on these materials as a function of magnetic field should be particularly interesting because of the occurrence of insulating (semiconducting) states in both AF and F phases. The resistivity of the AF phase should be larger than that of the F phase owing to the enhanced scattering of the electrons by the AF-aligned spins. Hence, the measurement of changes in resistivity as a function of magnetic field should provide evidence of contributions from spin scattering alone. (Note that for the manganese-containing compounds both spin scattering and contributions from conduction electrons set free by the establishment of the metallic state will contribute to the field-dependent resistivity.) In order to penetrate further into the origin of the CMR effect, it would be useful to concentrate on cases where only one of the components contributes.

C. Electronic structure

From the total density of states (DOS) for KCr_3O_8 in Fig. 4, it is evident that the P state with a finite DOS at the Fermi level (E_F) has metallic character. However, since the E_F falls on a peak of the DOS curve, stabilization in the P configuration is not favorable, in agreement with the total energy findings. Interestingly, the F state of KCr_3O_8 is insulating (semiconducting) with a band gap (E_g) of 0.31 eV. F insulators attract much attention owing to their potential application in spintronics devices. The presently studied compounds may be the first examples of Cr-containing oxides with F insulating behavior other than spinels. (Earlier, we[18] have predicted F insulating behavior in $Ca_2YCo_2O_6$ where Co takes the valence states Co^{II} and Co^{IV}.) Also in the AF configuration KCr_3O_8 is an insulator with a reduced E_g of 0.26 eV. A small energy gap (between −1.5 and −1.0 eV) is seen within the valence band (VB) of the F state, whereas the gap is somewhat larger (between −1.8 and −1.0 eV) in the AF state where more DOS is localized. The electronic structure of all the three compounds is similar in the sense that they have metallic character in the P state and insulating (semiconducting) character in the F and AF states. $NaCr_3O_8$ has $E_g=0.36$ eV in the F ground state and 0.41 eV in the (metastable, if at all realizable) AF state, whereas $RbCr_3O_8$ has $E_g=0.39$ eV in its AF ground state and 0.33 eV in the high-pressure F state.

As seen from Fig. 5, the K states are almost empty (scale multiplied by a factor of 10). This implies that K has donated almost all its electrons to oxygen and becomes ionic. Cr and O states are energetically degenerate implying strong cova-

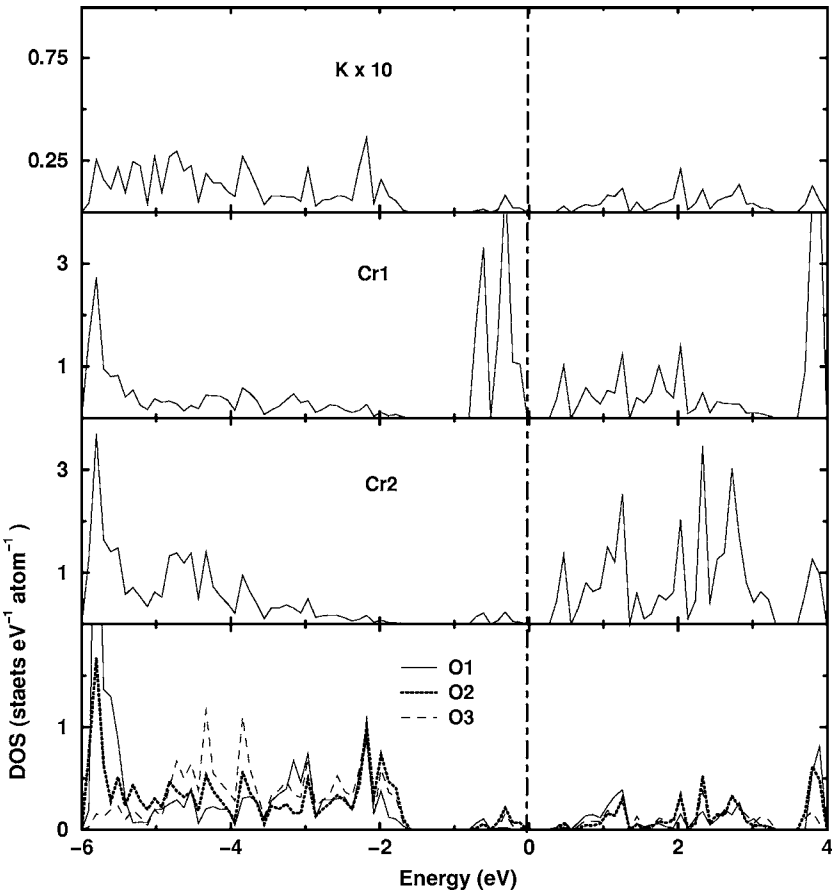

FIG. 5. Site-projected DOS for KCr_3O_8 in the antiferromagnetic state. The vertical line denotes the Fermi level (E_F).

lent interaction between them. The different valence states of the Cr ions are also obvious from their different DOS curves. The hybridization of the Cr2 *d* and O *p* states results in well-localized bonding states (−6 to −4 eV) in the VB and antibonding states in the conduction band (CB). Although the three different O atoms have states in the same energy region, they show significant topological differences in their DOS curves.

The partial DOSs for Cr1 and Cr2 are displayed in Fig. 6. As the contributions to the VB and CB from both Cr1 and

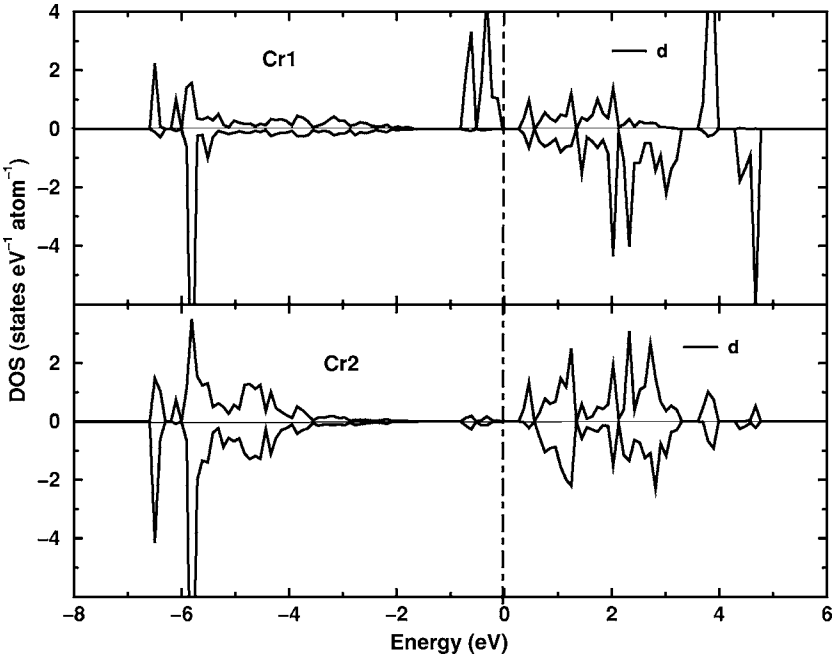

FIG. 6. Partial DOS of Cr1 and Cr2 in KCr_3O_8. The vertical line denotes E_F.

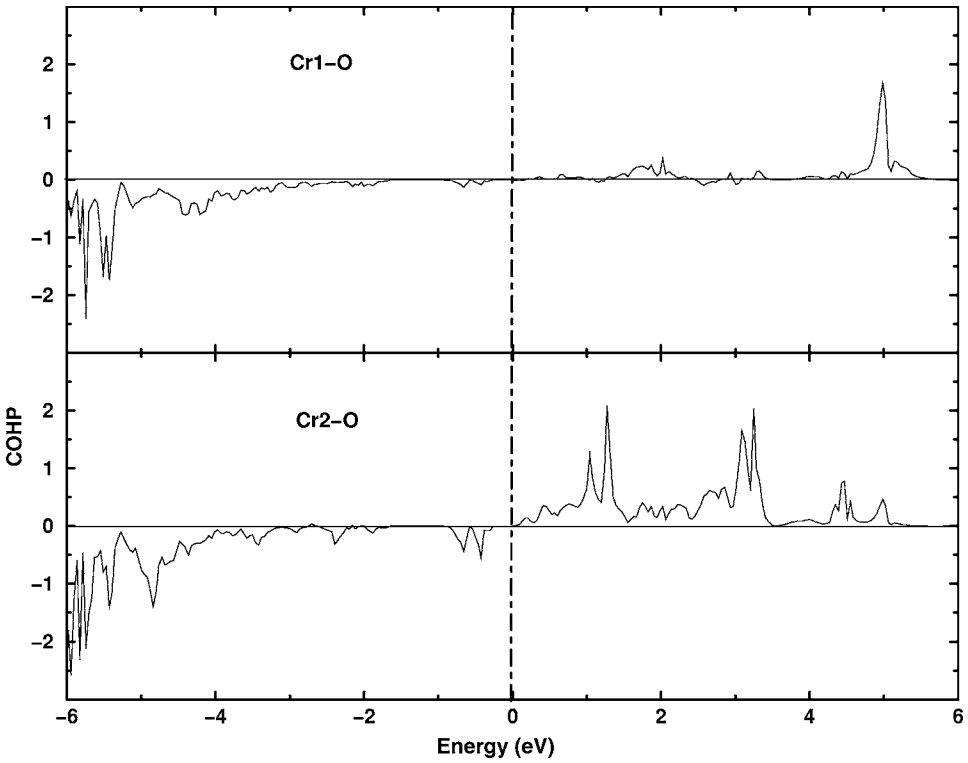

FIG. 7. Calculated COHP curves for Cr1 and Cr2 in KCr_3O_8. (The illustration refers strictly speaking to Cr1-O1 and Cr2-O2, but the profiles for Cr1-O3, Cr2-O2, and Cr2-O3 are very similar.) The vertical line denotes E_F.

Cr2 are mainly made up from *d* electrons (*s* and *p* are scarcely visible even after appreciable magnification) we here display only the *d*-electron DOS. The significant differences in the topology of the *d*-DOS curves and the integrated DOS values (4.2 states for Cr1 and 4.8 states for Cr2) reflect their different valence states. The majority-spin channel of Cr1 has more occupied states than its minority-spin channel. Moreover, if Cr2 really had been in the Cr^{VI} (d^0) state it should have an empty *d* band. Instead, it exhibits a considerable number of well-localized states with more or less equal occupancy in both spin channels. Hence it can be inferred that the almost-zero magnetic moment of Cr2 in these compounds is not due to a genuine Cr^{VI} (d^0) state, but results from negligible exchange splitting. The *lm*-projected DOS (not shown) also exhibits different occupancy of *d* orbitals for Cr1 and Cr2. As the studied systems have monoclinic crystal structure, the *d*-orbital splitting is not like that in a perfect cubic crystal field. After applying the proper rotation matrix, the octahedrally coordinated Cr1 does not exhibit perfect triply degenerate t_{2g} and doubly degenerate e_g orbitals. In the case of Cr1, the prominent peaks around −6 to −4 eV stem from t_{2g}-like orbitals whereas those closer to E_F come from e_g-like orbitals. The *lm*-projected DOS for Cr2 shows that all the *d* orbitals have almost equally filled majority- and minority-spin channels localized between −6 and −4 eV. Prominent peaks are seen for Cr1, Cr2, O1, and O3 in the energy range of −6 to −4 eV. This signals appreciable hybridization interaction between Cr and O.

D. Bonding characteristics

Crystal orbital Hamiltonian population (COHP, the DOS weighted by the corresponding Hamiltonian matrix elements) analysis[19,20] is a valuable tool to quantify the number of bonding and antibonding states. It may be recalled that a positive sign of the COHP indicates antibonding character and a negative sign bonding character. The calculated COHP for Cr1 and Cr2 is displayed in Fig. 7. For both kinds of Cr atoms the VB consists of bonding states and the CB of antibonding states indicating that both have strong bonding interaction with their surrounding O ions. The integrated COHP value (which provides a measure of bond strength) for Cr1 and Cr2 is 1.53 and 2.60 eV, respectively. Hence, the tetrahedral Cr2 atoms have stronger bonding interaction with its O neighbors than the octahedral Cr1 atoms consistent with the conclusion arrived from bond-length analysis.

A combined analysis of charge density, charge transfer, and electron localization function (ELF) plots gives additional insight into the bonding characteristics of solids.[21,22] A charge-density plot (distribution of charges in real space) together with a charge-transfer plot (difference between charge density of the solid and that of the atoms forming the solid) provides an overall idea about the transfer of charges involved in the formation of the solid. An ELF plot[23] helps to further characterize the different types of bonding involved, the ELF being defined between 0 and 1, and high values of ELF are found in covalent bonds and lone electron pairs.

As the DOS and COHP analyses clearly establish different valence states for Cr, we attempted to look for other signs of charge ordering through examination of charge-density plots [Fig. 8(a)]. For Cr1, charges are directed toward the octahedrally coordinated O ions, implying a degree of covalent Cr1-O interaction between them. In the case of Cr2, the charges are also directed toward the surrounding O ions, but here the charge is denser compared to those associated with Cr1, in agreement with the COHP analysis. The shorter Cr2-O bond length (1.62–1.69 Å) compared to the Cr1-O

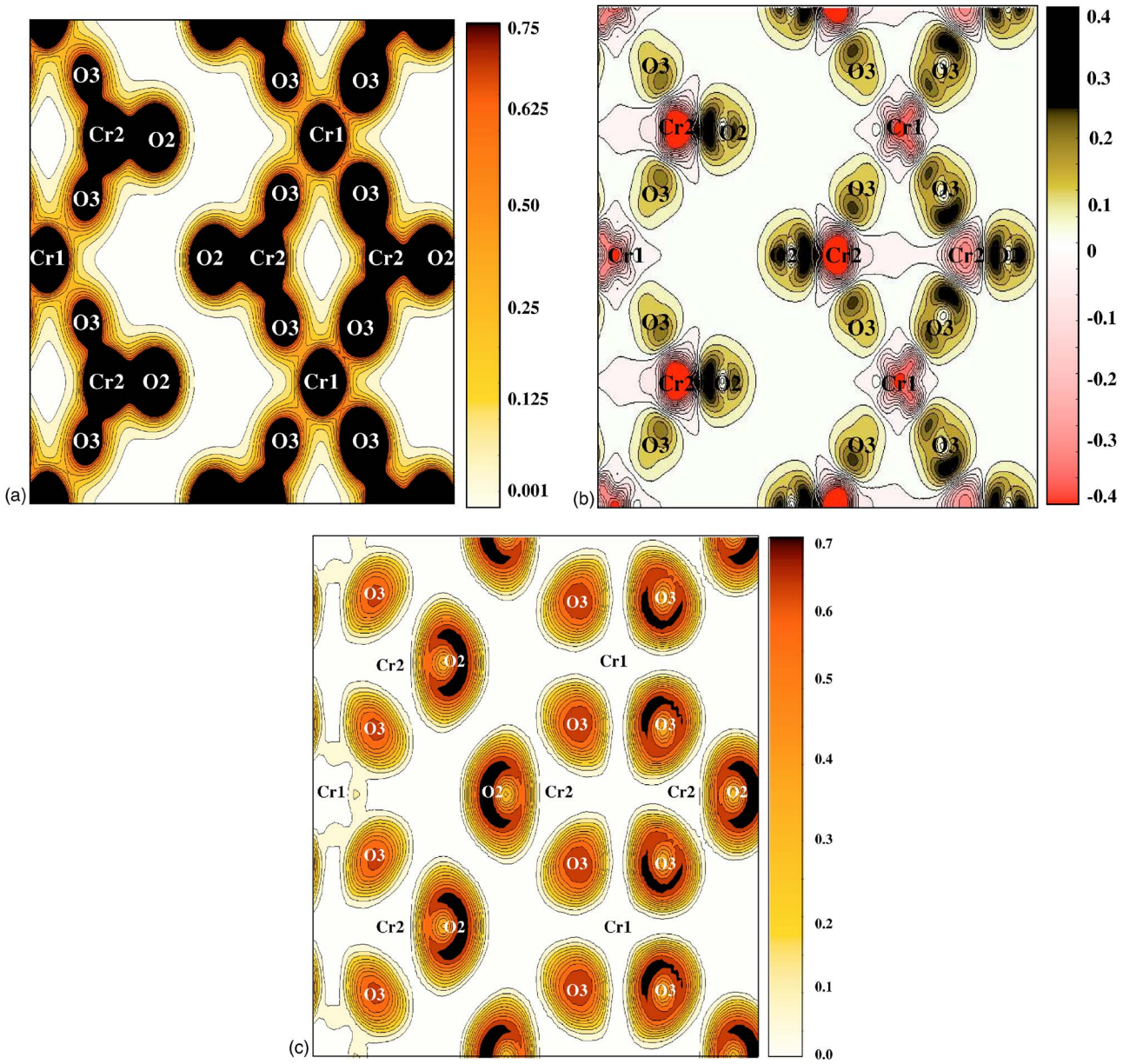

FIG. 8. (Color online) Plots in a,c plane of (a) charge density, (b) charge transfer, and (c) electron localization function for KCr_3O_8.

bond length (1.90–1.98 Å) and the enhanced charge density between Cr2 and O3 suggest strong covalent interaction. However, a closer look at the charge-transfer plot [Fig. 8(b)] paints a different picture. The anisotropic charge transfer from Cr1 to O3 implies that the Cr1-O3 bonds are of the coordinate covalent type where the shared electrons are supplied solely by Cr1. Moreover, Fig. 8(b) also shows transfer of charges from Cr2 to O3. If the Cr2-O3 bond only had covalent character, the charge-transfer plot should have shown positive charges between Cr2 and O3. However, the denser charge region between Cr2 and O3 in Fig. 8(a), does not imply a strong covalent bond (as customary thinking leads one to believe) but rather results from the presence of nonbonding *d* electrons on Cr2 (which are duly absent in the charge-transfer plot). Even though the ELF values for the Cr1-O and Cr2-O bonds [see Fig. 8(c)] are almost the same, the contours around the O3 atoms are directed toward Cr1 and away from Cr2. This suggests that the Cr1-O3 bond has some degree of directional character, whereas the Cr2-O3 bonds have both ionic and some degree of covalent character.

From the analyses of magnetic moments, *d*-orbital occupancies, and various means of bond characterization, it seems reasonable to conclude with Cr^{3+} as an approximate valence state for Cr1 whereas Cr^{6+} (as earlier studies have inferred) is certainly inappropriate for Cr2. Within the framework of the ionic picture it may be suggested that the actual charges associated with Cr2 should justify the label Cr^{2+} (with O^{1-} for all O atoms; Mulliken effective charges from the CRYSTAL03 program showed that O atoms have accepted around 0.9 electrons). The origin of the inferred deviation from the traditional formal valence scheme for charge allo-

cation (where adoption of 2− as the valence state for O forms a basic postulate) is the appreciable covalent contribution to the Cr2-O bonding.

V. CONCLUSION

It is predicted that a combination of ferromagnetic and insulating (at 0 K) behavior may be found in formally mixed-valent chromium compounds. The calculated structural parameters are in reasonable agreement with experimental values for $NaCr_3O_8$, KCr_3O_8, and $RbCr_3O_8$. The ground states of KCr_3O_8 and $RbCr_3O_8$ should exhibit antiferromagnetic insulating (semiconducting) behavior and on application of pressure a transformation to ferromagnetic-insulating (semiconducting) states is predicted. The energy difference between the antiferromagnetic and the ferromagnetic states of these compounds is very small. Hence, by application of a small magnetic field one can transform the antiferromagnetic-insulating (semiconducting) KCr_3O_8 and $RbCr_3O_8$ into ferromagnetic insulators (semiconductors). Experimental studies including magnetic, transport, and spectroscopic properties are recommended because these compounds are likely to exhibit exciting features.

ACKNOWLEDGMENTS

The authors are grateful to the Research Council of Norway for financial support and computer time at the Norwegian supercomputer facilities. The authors are grateful to Professor A. I. Liechtenstein for fruitful discussions on exchange parameters and R.V. wishes to acknowledge Arne Klaveness for his help.

*Electronic address: vidya.ravindran@kjemi.uio.no

[1] B. Raveau, A. Maignan, and C. Martin, J. Solid State Chem. **130**, 162 (1997).
[2] K.-A. Wilhelmi, Acta Chem. Scand. (1947-1973) **12**, 1958 (1965); Chem. Commun. (London) **1966**, 4371966.
[3] M. J. Saavedra, C. Parada, and E. J. Baran, J. Phys. Chem. Solids **57**, 1929 (1996).
[4] P. E. Blöchl, Phys. Rev. B **50**, 17953 (1994);G. Kresse and D. Joubert, *ibid.* **59**, 1758 (1999).
[5] G. Kresse and J. Furthmuller, Comput. Mater. Sci. **6**, 15 (1996).
[6] J. P. Perdew, K. Burke, and Y. Wang, Phys. Rev. B **54**, 16533 (1996);J. P. Perdew, K. Burke, and M. Ernzerhof, Phys. Rev. Lett. **77**, 3865 (1996).
[7] P. Vinet, J. H. Rose, J. Ferrante, and J. R. Smith, J. Phys.: Condens. Matter **1**, 1941 (1989).
[8] W. Klemm, Z. Anorg. Allg. Chem. **301**, 323 (1959).
[9] H. Fjellvåg (unpublished).
[10] U. Häussermann, H. Blomqvist, and D. Noréus, Inorg. Chem. **41**, 3684 (2002).
[11] P. Porta, M. Marezio, J. P. Remeika, and P. D. Dernier, Mater. Res. Bull. **7**, 157 (1972).
[12] A. I. Liechtenstein, M. I. Katsnelson, V. P. Antropov, and V. A. Gubanov, J. Magn. Magn. Mater. **67**, 65 (1987).
[13] V. I. Anisimov, F. Aryasetiawan, and A. I. Liechtenstein, J. Phys.: Condens. Matter **9**, 767 (1997).
[14] O. K. Andersen and O. Jepsen, Phys. Rev. Lett. **53**, 2571 (1984).
[15] J. B. Goodenough, *Magnetism and the Chemical Bond* (Interscience, New York, 1963).
[16] E. Konig, in *Magnetic Properties of Coordination and Organometallic Transition Metal Compounds*, edited by K. H. Hellwege, Landolt-Bornstein, New Series, Group II, Vol. 2 (Springer, New York, 1966).
[17] T. A. Hewston and B. L. Chamberland, J. Magn. Magn. Mater. **43**, 89 (1984).
[18] R. Vidya, P. Ravindran, H. Fjellvåg, A. Kjekshus, and O. Eriksson, Phys. Rev. Lett. **91**, 186404 (2003).
[19] R. Dronskowski and P. E. Blöchl, J. Phys. Chem. **97**, 8617 (1993).
[20] G. Krier, O. Jepsen, A. Burkhardt, and O. K. Andersen, computer code Tight Binding LMTO-ASA, Version 4.7 (Stuttgart, Germany, 1999).
[21] P. Ravindran, P. Vajeeston, R. Vidya, A. Kjekshus, and H. Fjellvåg, Phys. Rev. Lett. **89**, 106403 (2002).
[22] P. Vajeeston, P. Ravindran, R. Vidya, H. Fjellvåg, and A. Kjekshus, Phys. Rev. B **68**, 212101 (2003).
[23] A. Savin, R. Nesper, S. Wengert, and T. Fässler, Angew. Chem., Int. Ed. Engl. **36**, 1809 (1997).